Tendency of a rotating electron plasma to approach the Brillouin limit

Renaud Gueroult, Amnon Fruchtman, and Nathaniel J. Fisch

Citation: Phys. Plasmas **20**, 073505 (2013); doi: 10.1063/1.4816670
View online: http://dx.doi.org/10.1063/1.4816670
View Table of Contents: http://pop.aip.org/resource/1/PHPAEN/v20/i7
Published by the AIP Publishing LLC.

Tendency of a rotating electron plasma to approach the Brillouin limit

Renaud Gueroult,[1] Amnon Fruchtman,[2] and Nathaniel J. Fisch[1]
[1]*Princeton Plasma Physics Laboratory, Princeton University, Princeton, New Jersey 08543, USA*
[2]*Faculty of Sciences, H.I.T.-Holon Institute of Technology, Holon 58102, Israel*

(Received 15 February 2013; accepted 12 June 2013; published online 24 July 2013)

A neutral plasma is considered to be immersed in an axial magnetic field together with a radial electric field. If the electrons are magnetized, but the ions are not magnetized, then the electrons will rotate but the ions will not rotate, leading to current generation. The currents, in turn, weaken the axial magnetic field, leading to an increase in the rotation frequency of the slow Brillouin mode. This produces a positive feedback effect, further weakening the magnetic field. The operating point thus tends to drift towards the Brillouin limit, possibly finding stability only in proximity to the limit itself. An example of this effect might be the cylindrical Hall thruster configuration. © *2013 AIP Publishing LLC*. [http://dx.doi.org/10.1063/1.4816670]

I. INTRODUCTION

Many magnetic devices feature rapidly rotating clouds of electrons, including centrifugal fusion devices,[1–4] plasma centrifuge,[5–8] helicon source,[9] and various Hall-type thruster geometries.[10,11] In these configurations, the rotation is driven by crossed electric and magnetic fields.

In such configurations, the electron rotation frequency ω is in first approximation described by the azimuthal cross field drift velocity, in which case ω is assumed to be equal to $E(Br)^{-1}$, with E the electric field intensity, B the magnetic field intensity, and r the radial coordinate. A more complete description indicates that, when the magnetic field is inclined with respect to the radial direction, the radial centrifugal force exerted on the azimuthally rotating electron cloud has components both parallel to the magnetic field line (and compensated therefore by a parallel electric field) and perpendicular to the magnetic field.[12] The perpendicular component of the centrifugal force results in an additional azimuthal drift, which modifies the rotation frequency.[1] The rotation frequency ω is therefore no longer equal to $E(Br)^{-1}$, but some particular kind of Brillouin solution (see, *e. g.*, Ref. 13) generalized to non-purely axial magnetic fields. This deviation is shown[1] to be negligible for $E(Br)^{-1} \ll \omega_c$, where ω_c is the electron gyro-frequency, but becomes non negligible when these two frequencies are comparable.

The particular feature that we uncover here is the rather fascinating tendency, through a feedback mechanism, of the rotating electron cloud flow to grow closer to the so-called Brillouin limit.[14] In this limit, the frequency of rotation of the electron cloud becomes one half of the electron gyro-frequency. This tendency is shown to occur for a particular set of plasma parameters, such as observed, for example, downstream of the miniaturized cylindrical Hall thruster (CHT).[15]

The paper is organized as follows: In Sec. II, the role played by the non negligible induced magnetic field on the electron cloud azimuthal rotation frequency is introduced. In Sec. III, a simplified geometrical configuration is used to derive analytical solutions for the rotation frequency under the assumption of a solid body rotation. In Sec. IV, different electron cross-field transport regimes are discussed. In Sec. V, these considerations are applied, as an example, to data obtained in the cylindrical Hall thruster. In Sec. VI, the main findings are summarized.

II. FEEDBACK LOOP CAUSED BY THE INDUCED MAGNETIC FIELD

Under the assumption of a purely homogeneous axial magnetic field $\boldsymbol{B} = B_0\hat{\boldsymbol{z}}$ and a radial electric field $\boldsymbol{E} = -E_0\hat{\boldsymbol{r}}$ $(E_0 > 0)$, and neglecting initially the induced magnetic field, the electron azimuthal rotation frequency $\omega(r)$ can be shown to be the slow Brillouin rotation mode[13]

$$\omega^- = \frac{eB_0}{2m}\left[1 - \sqrt{1 - 4\frac{mE_0}{eB_0^2 r}}\right]. \tag{1}$$

In principle, another solution for the rotation frequency would be the fast Brillouin rotation mode

$$\omega^+ = \frac{eB_0}{2m}\left[1 + \sqrt{1 - 4\frac{mE_0}{eB_0^2 r}}\right]. \tag{2}$$

However, since the rotation of an electron in the fast mode $\omega(r) = \omega^+$ requires a significantly larger electron initial kinetic energy, only a negligible fraction of electrons will actually orbit in this mode, so that the contribution of these electrons can be reasonably neglected. The slow rotation mode $\omega(r) = \omega^-$ will therefore be the only one considered in the rest of the paper.

Consider a homogeneous electron density n_e rotating at the frequency $\omega(r) = \omega^-$ as obtained in Eq. (1). The induced magnetic field $\boldsymbol{B_i} = -B_i\hat{\boldsymbol{z}}$ can then be estimated as

$$B_i = \int_r^{r_0} e\mu_0 n_e \omega(r') r' dr', \tag{3}$$

with r_0 the external radius of the device and μ_0 the free space permeability. A lower estimate of B_i can be obtained by noting that, as shown in Eq. (1), ω is always larger than $E(B_0 r)^{-1}$, which yields

$$B_i \geq e\mu_0 n_e \frac{E_0}{B_0}(r_0 - r). \tag{4}$$

Introducing the plasma frequency $\omega_p^2 = e^2 n_e (m\epsilon_0)^{-1}$, the speed of light $c = (\epsilon_0\mu_0)^{-1/2}$, and the parameter $p_0 = mE_0/(eB_0^2 r)$ representative of the proximity of the vacuum fields conditions to the Brillouin limit, Eq. (4) can be rewritten as

$$\frac{B_i}{B_0} \geq \frac{\omega_p^2}{c^2} r_0^2 \left(1 - \frac{r}{r_0}\right)\frac{r}{r_0} p_0 = \left(\frac{r_0}{\delta_s}\right)^2 \left(1 - \frac{r}{r_0}\right)\frac{r}{r_0} p_0, \tag{5}$$

where $\delta_s = c/\omega_p$ is the electron skin depth. The condition for a non negligible induced magnetic field can then be seen as the combination of two factors. The first factor is the ratio of the plasma column radius over the electron skin depth. The second one is the parameter p_0, with $p_0 = 1/4$ at the Brillouin limit for which $\omega/\omega_c = 1/2$. Equation (5) indicates that the induced magnetic field is to be expected to play a non negligible role when the product of these factors is $\mathcal{O}(1)$. Let us consider in the remaining of this paper the situation for which such a condition is met.

The non-negligibility of the induced magnetic field B_i demands considering the effective magnetic field B in place of the externally applied magnetic field B_0 in Eq. (1). Since the induced magnetic field depends itself on the rotation frequency ω, a feedback loop exists. The magnetic field weakening modifies the rotation frequency, which itself modifies the magnetic field strength through the induced magnetic field. The system to be solved is then

$$\omega = \frac{eB}{2m}\left[1 - \sqrt{1 - 4\frac{mE}{eB^2 r}}\right], \tag{6a}$$

$$B = B_0 - \int_r^{r_0} e\mu_0 n_e \omega(r') r' dr'. \tag{6b}$$

The derivation of solutions for Eq. (6) requires additional assumptions as for the electric field E and the magnetic field B (or the rotation frequency ω), as well as for the electron number density n_e.

III. RIGID ROTOR

In order to quantify the effect of the magnetic field weakening on the electron cloud rotation speed, an analytical solution for Eq. (6) can be obtained in the idealized case corresponding to the rigid rotor rotation (ω independent of r) of a uniform electron cloud (n_e constant). Equation (6) then becomes

$$\omega = \frac{eB}{2m}\left[1 - \sqrt{1 - 4\frac{mE}{eB^2 r}}\right], \tag{7a}$$

$$B = B_0 - \frac{e\mu_0 n_e}{2}(r_0^2 - r^2)\omega. \tag{7b}$$

Introducing the dimensionless variables

$$\xi := \frac{r}{r_0}, \tag{8a}$$

$$\Omega_c(\xi) := \frac{\omega_c(\xi)}{\omega_{c_0}}, \tag{8b}$$

$$\omega_c := \frac{eB}{m}, \tag{8c}$$

$$\omega_{c_0} := \frac{eB_0}{m}, \tag{8d}$$

$$\Omega := \frac{\omega}{\omega_{c_0}}, \tag{8e}$$

$$a(\xi) := \frac{eE(\xi)}{m\omega_{c_0}^2 r_0}, \tag{8f}$$

$$s := \frac{\omega_p^2}{c^2} r_0^2, \tag{8g}$$

Equation (7) reads

$$\Omega = \frac{\Omega_c}{2}\left[1 - \sqrt{1 - 4\frac{a}{\Omega_c^2 \xi}}\right], \tag{9a}$$

$$\Omega_c = 1 - \frac{s}{2}(1 - \xi^2)\Omega. \tag{9b}$$

The variables a and Ω_c are the dimensionless electric and magnetic fields, s is the dimensionless electron number density responsible for the diamagnetic effect, and Ω is the resulting dimensionless uniform rotation angular frequency.

Rewriting Eq. (9a), one obtains that the dimensionless electric field must satisfy

$$a = \Omega\xi(\Omega_c - \Omega). \tag{10}$$

Plugging in the expression for the dimensionless magnetic field Ω_c obtained from Eq. (9b), the explicit dependence of the electric field on the radial coordinate reads

$$a = \Omega\xi\left[1 - \frac{s}{2}(1 - \xi^2)\Omega - \Omega\right]. \tag{11}$$

It is clear that the electric field does not depend linearly on the radial coordinate ξ as obtained when neglecting the induced magnetic field. The corresponding dimensionless potential v is

$$v := \int_0^{\xi} a d\xi' = \frac{e}{mr_0^2\omega_{c_0}^2}\phi = \Omega\left[\frac{\xi^2}{2} - \frac{s}{2}\left(\frac{\xi^2}{2} - \frac{\xi^4}{4}\right)\Omega - \frac{\xi^2}{2}\Omega\right], \tag{12}$$

with ϕ the potential at distance r relative to the axis. The dimensionless voltage across the electron cloud is then

$$v_0 := \int_0^1 a d\xi' = \frac{e}{mr_0^2\omega_{c_0}^2}\phi_0 = \frac{\Omega}{2}\left[1 - \Omega\left(1 + \frac{s}{4}\right)\right]. \tag{13}$$

The uniform rotation frequency Ω can consequently be interpreted as a function of the two dimensionless parameters v_0 and s. Solving Eq. (13), one gets

$$\Omega^{\pm} = \frac{1 \pm \sqrt{1 - 8v_0(1+s/4)}}{2(1+s/4)}. \tag{14}$$

From energetic considerations, the naturally arising mode is $\Omega = \Omega^{-}$. We verify that, in the limit case of a negligible electron density $s \to 0$, Eq. (14) is equivalent to the classical slow Brillouin rotation mode driven by an applied voltage $\phi = \phi_0 \xi^2$. The classical Brillouin flow limit $v_0 \leq 1/8$ is here modified by the diamagnetic effect through the dimensionless electron density s, with

$$8v_0\left(1 + \frac{s}{4}\right) \leq 1, \tag{15}$$

or in dimensional form

$$\frac{8m\phi_0}{eB_0^2 r_0^2}\left(1 + \frac{\mu_0 e^2 n_e r_0^2}{4m}\right) \leq 1. \tag{16}$$

Figure 1(a) shows the evolution of Ω as a function of the dimensionless variables s and v_0. The deviation from the neglected induced magnetic field case is, as expected, materialized by an increase in Ω for large values of s, or in other words for large electron number densities (see Fig. 1(b)). This result is however insufficient to quantify the proximity of the operating conditions to the Brillouin flow limit since the gyro-frequency is itself decreasing as the induced magnetic field increases.

Once the rotation frequency Ω is determined, the dimensionless magnetic field Ω_c can be derived as a function of the same dimensionless variables s and v_0,

$$\Omega_c = 1 - \frac{s}{2}(1-\xi^2)\Omega = 1 - \frac{1 - \sqrt{1 - 8v_0(1+s/4)}}{4(1+s/4)}(1-\xi^2)s. \tag{17}$$

The magnetic field radial profiles obtained for various dimensionless electron number densities and a dimensionless electric potential $v_0 = 0.043$ are plotted in Fig. 2(a). The field weakening is seen to be significant close to the axis, with a 30% decrease at $\xi = 0.5\,(r = r_0/2)$ for $s \geq 5.7$. Insight of the operating conditions' proximity to the Brillouin flow limit can be obtained by analyzing the radial dependence of the ratio Ω/Ω_c, the Brillouin parameter, as plotted in Fig. 2(b). As a matter of fact, from Eq. (9a), the Brillouin flow limit is equivalent to $\Omega/\Omega_c = \omega(\xi)/\omega_c(\xi) = 1/2$. If neglecting the induced magnetic field, $\Omega = (1 - \sqrt{1 - 8v_0})/2$ and $\Omega_c = 1$. Figure 2(b) together with Fig. 2(a) clearly demonstrates the role of diamagnetism on the evolution towards to the Brillouin flow. The magnetic field weakening within the core of the plasma indeed corresponds to a large increase in the Brillouin parameter, with Ω/Ω_c increasing rapidly towards the 1/2 limit in response to an electron number density increase past a given value.

We note that even larger electron number densities (larger s values) would yield a deconfinement ($p = mE/(eB^2 r) \geq 1/4$) of the electrons. More specifically, looking at Eq. (14), one can show that the dimensionless rotation frequency at the Brillouin limit is

$$\Omega = \frac{1}{2(1+s/4)}, \tag{18}$$

so that on axis

$$\frac{\Omega}{\Omega_c(\xi=0)} = \frac{1}{2}, \tag{19}$$

while at the edge of the plasma, $\Omega_c(\xi = 1) = 1$, and

$$\frac{\Omega}{\Omega_c(\xi=1)} = \frac{1}{2(1+s/4)} \leq \frac{1}{2}. \tag{20}$$

A dense plasma could therefore become unstable close to the axis while the outer regions remain stable, leading in turn to the formation of a hollow cylindrical plasma.

Another quantity of interest is the ratio of rotational to electrostatic energy (relative to the axis)

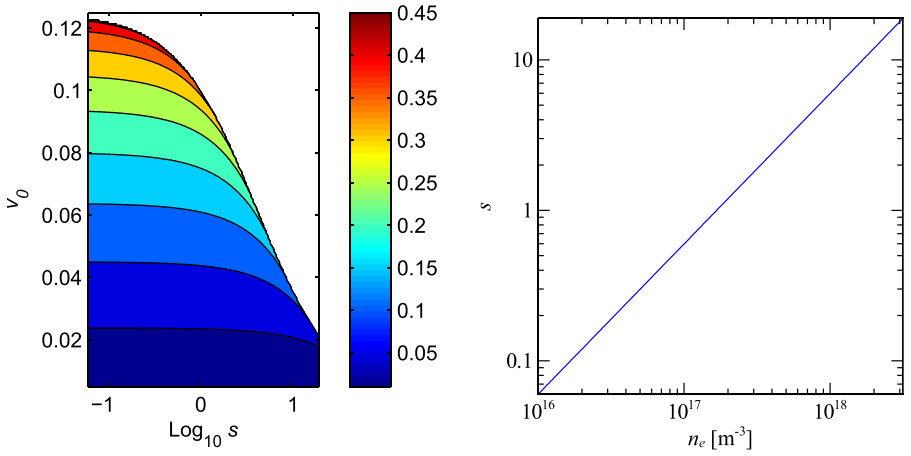

(a) $\Omega(s, v_0)$ (b) $s \sim 6\ 10^{-18} n_e[\mathrm{m}^{-3}]$

FIG. 1. Map of the uniform dimensionless rotation frequency $\Omega = \omega/\omega_{c_0}$ as a function of the dimensionless electron number density s and electric potential v_0 (a). The dependence of s over n_e is indicated in (b), with $s \sim 6\ 10^{-18} n_e[\mathrm{m}^{-3}]$ for $r_0 = 13\,\mathrm{mm}$.

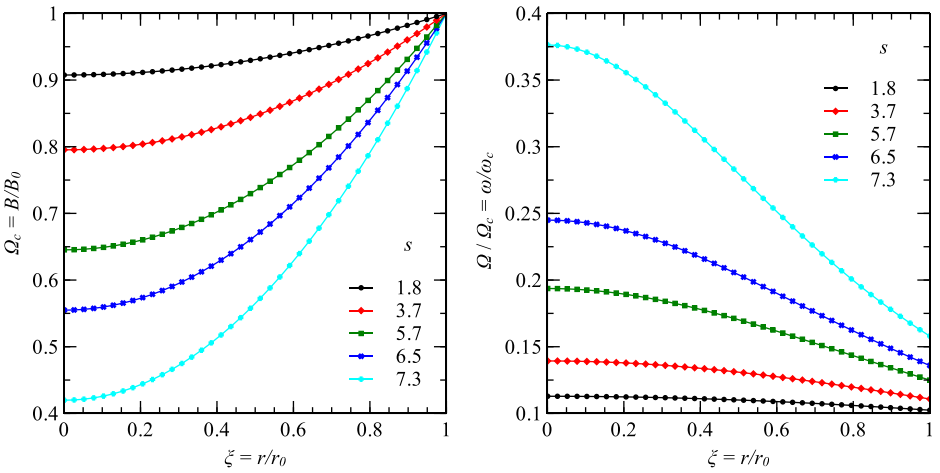

(a) $\Omega_c(\xi)$ (b) $\Omega/\Omega_c(\xi)$

FIG. 2. Magnetic field (a) and Brillouin parameter (b) radial profiles for various values of the dimensionless electron number density s and a dimensionless electric potential $v_0 = 4.3\ 10^{-2}$ ($E_0(r_0) \sim 2\ 10^4$ V.m^{-1}).

$$\chi := \frac{m}{2}\frac{\omega^2 r^2}{e\phi}. \tag{21}$$

Using the expression for the potential,

$$\frac{e\phi}{\omega_{c_0}^2 m r_0^2} = \Omega\left[\frac{\xi^2}{2} - \frac{s}{2}\left(\frac{\xi^2}{2} - \frac{\xi^4}{4}\right)\Omega - \Omega\frac{\xi^2}{2}\right], \tag{22}$$

one gets

$$\chi(\xi) = \frac{\omega_{c_0}^2 m r_0^2}{2e\phi}\Omega^2\xi^2 = \frac{\Omega}{\left[1 - s\left(\frac{1}{2} - \frac{\xi^2}{4}\right)\Omega - \Omega\right]}. \tag{23}$$

The ratio χ increases monotonically with ξ. Therefore, its maximal value is

$$\chi_{\max} = \frac{\Omega}{[1 - \Omega(1 + s/4)]}. \tag{24}$$

Substituting the slow mode dimensionless rotation frequency Ω as specified by Eq. (14), it yields,

$$\chi_{\max} = \frac{1 - \sqrt{1 - 8v_0(1 + s/4)}}{(1 + s/4)[1 + \sqrt{1 - 8v_0(1 + s/4)}]} \leq 1. \tag{25}$$

The stronger the diamagnetic effect, the larger the rotational to electrostatic energy ratio. At the limit of zero density, $s = 0$, the rotational energy becomes equal to the electrostatic energy if $8v_0 = 1$, that is, to say at the Brillouin limit. For a vanishing s, it occurs at $\Omega = 1/2$, in which case the ratio is then identically unity across all the cylinder:

$$\chi(\xi) = \frac{\Omega}{1 - \Omega}. \tag{26}$$

The assumption of a solid body rotation is mainly motivated by the interest for the possibility of an analytical solution. The physical realizability of these solutions is therefore not immediate. But this idealized case highlights a trend, which could be checked computationally for more realistic models.

IV. CROSS-FIELD TRANSPORT

Recalling the modeling of the purely axial magnetic field configuration, the assumption of a particular transport regime can be rewritten as a given relation between the electric and magnetic fields E and B. More specifically, the assumption of a constant discharge current across the field lines, that is, to say of a constant radial current in our idealized case, leads to the invariance of the product σE, where σ is the plasma conductivity. Since the two different transport regimes considered above can be rewritten as $\sigma \propto B^{-1}$ (Bohm scaling) or $\sigma \propto B^{-2}$ (classical diffusion), a constant conductivity yields, respectively, $E \propto B$ or $E \propto B^2$.

Equation (6) is consequently numerically solved for various dependences of the electric field E on the magnetic field B. The system is solved iteratively, starting from the initial magnetic field and electric potential

$$\boldsymbol{B}^{(0)} = B_0\hat{\boldsymbol{z}}, \tag{27a}$$

$$\boldsymbol{\phi} = \phi_0\frac{r^2}{r_0^2}, \tag{27b}$$

until the relative error with respect to the magnetic field B converges within one percent. The corresponding initial electric field can be expressed as a function of the variable v_0 defined in Eq. (13), with

$$\boldsymbol{E}^{(0)} = -\frac{2eB_0^2}{m}v_0 r\hat{\boldsymbol{r}}. \tag{28}$$

Let us first consider Bohm scaling for the electron cross-field transport, for which E is assumed proportional to B, $E = E^{(0)}B/B^{(0)}$. Fig. 3 shows that the dimensionless rotation frequency Ω evolution is qualitatively similar to the rigid rotor solution presented in Sec. III. The main difference lies in the radial dependence of the rotation frequency, with Ω comparable to the rigid rotor values close to the axis, and globally smaller at larger radial positions. The regime for which the operating conditions are close to the Brillouin flow is in this case shifted to larger electron number density (larger s values), as illustrated in Fig. 4.

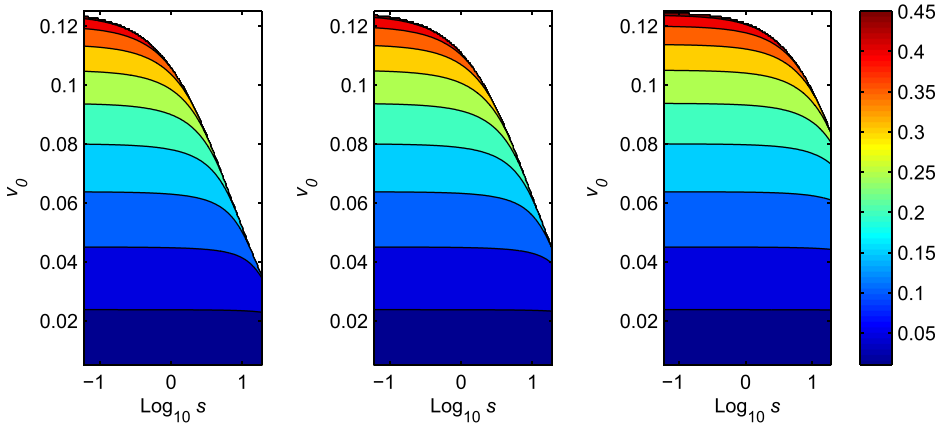

(a) $\xi = 1/3$ (b) $\xi = 2/3$ (c) $\xi = 1$

FIG. 3. Map of the dimensionless rotation frequency $\Omega = \omega/\omega_{c_0}$ as a function of the dimensionless electron number density s and electric potential v_0 in case of a Bohm scaling ($E = E^{(0)}B/B^{(0)}$) for various normalized radial positions ξ. $\xi = 1/3$ (a), $\xi = 2/3$ (b), and $\xi = 1$ (c).

Consider now the limiting case of a negligible dependence of the conductivity on the magnetic field, i e., a regime for which the electric field E is supposed independent of B. In this limit, the numerical solutions plotted in Fig. 4 confirm the general trend previously identified. The main difference consists in a shift towards lower values of the electron number density for which the operating conditions reach a given proximity to the Brillouin flow (*e.g.* a given $\Omega/\Omega_c(\xi)$), the sudden increase in $\Omega/\Omega_c(\xi)$ occurring for approximately half the electron number density observed in case of a Bohm scaling ($n_e \sim 9\ 10^{17}\,\mathrm{m}^{-3}$).

Consider also the classical electron cross-field regime, for which the electric field is assumed proportional to the square of the magnetic field, $E \propto B^2$. Equation (6) then indicates a stabilizing feedback loop, since an increase in the magnetic field B would yield an increase in the angular frequency, which itself would weaken the magnetic field. The rotation frequency ω is therefore expected to remain close to its free space value under the assumption of a classical electron cross-field transport.

To summarize, with the exception of the classical electron cross-field transport, the various regimes studied highlight a tendency of the electron rotating cloud to grow toward the Brillouin limit much similar to the one identified in the case of the analytical rigid-rotor model presented in Sec. III. In addition, despite small variations, the conditions for which this growth is observed remain globally identical (within roughly a factor 2.5). These descriptions do rely on the simplifying assumption of constant electron number density. The dependence of the electron number density on the rotation frequency, as well as the implications with respect to the results obtained, is discussed in Appendix A.

V. EXAMPLE: CYLINDRICAL HALL THRUSTER

The CHT is a promising alternative to the conventional annular Hall Thruster (HT) particularly in scaling to low power.[15] A number of variations of Hall thrusters with large axial field components have now been explored as well.[16–19] In this open or magnetic-nozzle configuration, the outer part of the central portion of a conventional HT annular channel is eliminated, giving a larger volume to surface ratio for a given thruster radial dimension. The electron losses to the walls are therefore smaller, and it stands to reason that so might be the erosion.

However, because of the partial elimination of the central annular channel, the magnetic field lines have a significantly larger component in the axial direction as compared with the magnetic field lines in the conventional HT. Thus, while there are many magnetic field effects, such as magnetic mirroring or focusing exhibited by the conventional

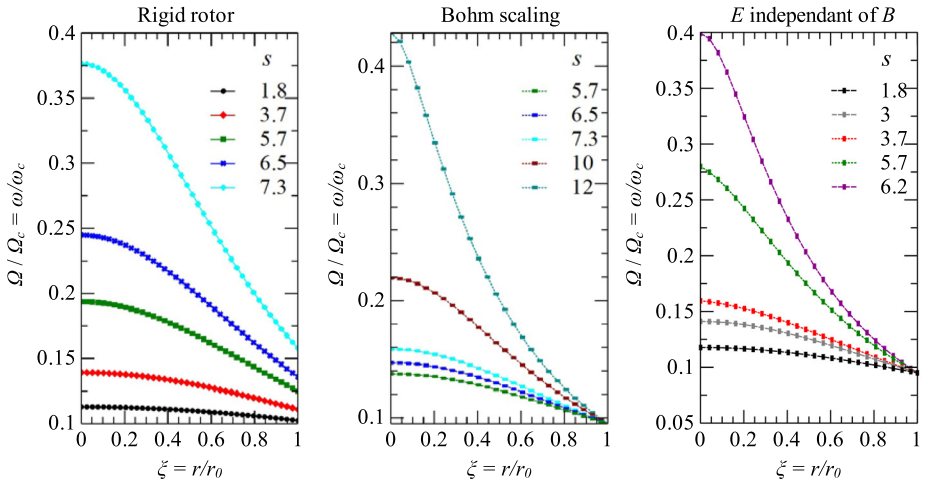

FIG. 4. Proximity to the Brillouin flow for various s values and electron-cross field regimes. The Brillouin flow regime corresponds to $\Omega/\Omega_c(\xi) = 1/2$. The weaker the electron cross field diffusion, the larger the electron number density required to yield a deviation from the neglected induced magnetic field case.

TABLE I. Dimensions and typical operating conditions downstream of a miniaturized cylindrical Hall thruster, from Refs. 12 and 22.

Parameter	Value
Distance from axis [mm]	13
Potential relative to axis [V]	130
Magnetic field [T]	0.01
Electron number density [m^{-3}]	10^{18}

annular thruster,[18–21] that may be expected to be found also in cylindrical Hall thrusters, cylindrical thrusters may exhibit new features or exaggerated features compared with conventional annual thrusters. One such example is the role of the diamagnetic effect described in this paper.

We apply the analysis described above to the miniaturized thruster described in Refs. 22 and 12. Table I presents values of parameters downstream that CHT. For $n_e = 10^{18}\,\mathrm{m}^{-3}$, the electron skin depth δ_s is about 5 mm, that is, to say about a third of the channel width. In addition, the vacuum electric E_0 and magnetic field B_0 values give $p_0 \sim 0.08$ at $r = r_0/2$, so that according to Eq. (5), one gets $B_i/B_0 \geq 0.15$. Consequently, the derivation of the electron cloud rotation frequency downstream of this CHT indeed requires computing the effect of the induced magnetic field. Taking the voltage $\phi_0 = 130\,\mathrm{V}$, the dimensionless voltage is $v_0 = 0.043$ while the dimensionless electron number density is $s = 6$. The dimensionless rotation frequency is then $\Omega = 0.125$, considerably smaller than unity. However, as a result of the large diamagnetic current, we obtain for the rigid-rotor flow a much larger ratio within the plasma core, with $\Omega/\Omega_c \geq 0.2$ for $\xi \leq 0.5$. The fact that the results obtained for the classical diffusion model (cf. Sec. IV) and typical CHTs' parameters are consistent with these values is taken as a strong indicator that the diamagnetism effects previously discussed are likely to be observed downstream of a cylindrical Hall thruster.

Closer to the anode of the CHT, the diamagnetic effect is weaker. However, each electron is expected to bounce back and force between the anode region and the downstream region, and therefore it experiences being closer to the Brillouin limit along its trajectory downstream from the anode. It is true that downstream from the anode the magnetic field lines diverge and the validity of the approximation of an axial magnetic field is therefore only limited. However, some of the flow behavior, such as the existence of two solid rotation frequencies exists also when the magnetic field is divergent.[23]

VI. SUMMARY

In this paper, the effects of diamagnetism on the rotation of an electron cloud within a neutral plasma in which electrons are magnetized, but ions are not magnetized, are addressed. In such configurations, typically obtained by cross electric and magnetic fields, the rotation of the sole electron component can yield large currents, which in turn weaken the axial magnetic field. For some particular conditions, this magnetic field weakening is shown to be non negligible. In this case, the rotation frequency of the slow Brillouin mode increases as a result of the magnetic field decrease, producing a positive feedback effect.

For solid body rotation of a homogeneous electron cloud, analytical solutions for the rotation frequency are derived for an idealized magnetic field topology. These solutions demonstrate a significant diamagnetism effect for larger electron number densities, which tends to bring the operating point closer to the Brillouin limit. This trend is confirmed by substituting for solid body rotation different assumptions representative of different electron cross-field transport regimes, and numerically solving for the rotation frequency. The proximity to the Brillouin flow limit is seen to be greater for large cross-field transport regimes, such as Bohm scaling, while classical diffusion maintains the system further away from this limit.

Consideration of the typical operating parameters reported downstream of a cylindrical Hall thruster reveals that such diamagnetic effects are likely to be locally observed in these thrusters. The resulting magnetic field in the core of the plasma is expected to be significantly weaker than its vacuum field value, exhibiting locally an electron flow close to the Brillouin limit. Experimental measurements of the electron rotation speed, or alternatively a mapping of the in-operation magnetic field, should corroborate this analysis. Since the magnetic field topology is expected to deviate from its vacuum shape, a significant modification of the electric potential distribution in the thruster is anticipated. This electric potential remapping is likely to affect significantly the ion beam focusing in a miniaturized cylindrical Hall thruster.

ACKNOWLEDGMENTS

This work was supported by US DOE under Contract Nos. DE-FG02-06ER54851 and DE-AC02-09CH11466, and by the US-Israel Binational Science Foundation under Grant No. 2008224.

APPENDIX A: FEEDBACK THROUGH IONIZATION

The solid body rotation model presented in Sec. III, as well as the simulations presented in Sec. IV, indicates a relatively sudden appearance of the diamagnetism effects above a threshold electron number density. Because of this electron number density sensitivity, it seems suitable to depict how the relaxation of the constant electron density hypothesis would alter these results. A solution consists in modeling the electron impact ionization cross-section σ dependence on the rotation frequency. Since the electron cloud rotation is expected to be supersonic, the ionization rate will be determined by the electron rotation velocity. More specifically, an increase in the rotation frequency yields an electron kinetic energy $\varepsilon_c = m\omega^2 r^2/2$ increase, modifying in turn the ionization rate $\sigma n_g v$, where $v = \omega r$ is the electron velocity and n_g is the background neutral number density. In addition, assuming solid body rotation, the kinetic energy of an electron close to the outer wall will be much larger than the one of an electron in the central region, leading to an inhomogeneous ionization rate.

Above some threshold kinetic energy, an electron becomes less efficient at ionizing background neutrals. Consequently, two cases can be set apart depending on the scaling of the rotational energy with respect to the electron kinetic energy ε_i for which the electron impact ionization rate peaks. On the one hand, if $\varepsilon_c > \varepsilon_i$, an increase in the rotation frequency ω with respect to its free space value $\omega_0 = eB_0[1 - \sqrt{1 - 4p_0}]/(2m)$ will result in an increase in electron number density n_e. This feedback loop would consequently bring the system even closer to the Brillouin limit. On the other hand, if $m(\omega r)^2/2 < \varepsilon_i$, an increase in the rotation frequency would yield a decrease in the electron number density, stabilizing in turn the system.

A hint of the behavior likely to appear in the cylindrical Hall thruster configuration discussed in Sec. V can be obtained as follows. The rotation frequency corresponding to the Brillouin flow limit is $\omega_c/2$, which is equivalent to an electron energy $\varepsilon_B = e^2B^2r^2/(8m)$ for solid body rotation of the electron cloud. An upper limit for this electron energy ε_e can be calculated at the outermost radial position r_0 by neglecting the induced magnetic field. Considering the typical miniaturized CHT parameters summarized in Table I, one gets $\varepsilon_B \leq 370\,\text{eV}$. Using, as an example, the cross section in Xenon,[24] the kinetic energy above which an electron becomes less efficient at ionizing background neutrals is $\varepsilon_i \sim 320\,\text{eV}$. These two energies ε_B and ε_i being comparable, an increase in the rotation frequency ω will result in an increase in electron number density n_e in most of the domain. Such an n_e increase will globally strengthen the induced magnetic field, amplifying in turn the feedback loop exhibited by Eq. (7). A possible exception consists of the limited regions where the conditions are already sufficiently close to the Brillouin flow for the electron energy to be larger than ε_i. In such regions, an increase in the rotation frequency will yield an electron density decrease, giving a stabilizing effect. Note however that additional effects, in particular, collisions, should generally lower the electron energy, so that it remains much lower than ε_i.

Thus, with the exception of particularly large rotation frequencies, the consideration of the rotation frequency's influence on the electron number density is expected to lead to predicting an even stronger feedback loop, bringing the system even more quickly towards the Brillouin limit. It is worth noting that this process is expected to take place irrespectively of the transport regime.

[1]B. Lehnert, Nucl. Fusion **11**, 485 (1971).
[2]Y.-M. Huang and A. B. Hassam, Phys. Rev. Lett. **87**, 235002 (2001).
[3]V. Volosov, Nucl. Fusion **46**, 820 (2006).
[4]A. J. Fetterman and N. J. Fisch, Phys. Rev. Lett. **101**, 205003 (2008).
[5]M. Krishnan, M. Geva, and J. L. Hirshfield, Phys. Rev. Lett. **46**, 36 (1981).
[6]T. Ohkawa and R. L. Miller, Phys. Plasmas **9**, 5116 (2002).
[7]A. J. Fetterman and N. J. Fisch, Phys. Plasmas **18**, 094503 (2011).
[8]R. Gueroult and N. J. Fisch, Phys. Plasmas **19**, 122503 (2012).
[9]T. Lafleur, K. Takahashi, C. Charles, and R. W. Boswell, Phys. Plasmas **18**, 080701 (2011).
[10]A. Morozov, Plasma Phys. Rep. **29**, 235 (2003).
[11]A. Fruchtman, N. J. Fisch, and Y. Raitses, Phys. Plasmas **8**, 1048 (2001).
[12]N. J. Fisch, Y. Raitses, and A. Fruchtman, Plasma Phys. Controlled Fusion **53**, 124038 (2011).
[13]R. C. Davidson, *Physics of Nonneutral Plasmas* (Imperial College Press, 2001).
[14]L. Brillouin, Phys. Rev. **67**, 260 (1945).
[15]Y. Raitses and N. J. Fisch, Phys. Plasmas **8**, 2579 (2001).
[16]A. Shirasaki and H. Tahara, J. Appl. Phys. **101**, 073307 (2007).
[17]N. A. MacDonald, M. A. Cappelli, S. R. Gildea, M. Martinez-Sanchez, and W. A. Hargus, Jr., J. Phys. D: Appl. Phys. **44**, 295203 (2011).
[18]R. R. Hofer, R. S. Jankovsky, and A. D. Gallimore, J. Propul. Power **22**, 721 (2006).
[19]J. A. Linnell and A. D. Gallimore, Phys. Plasmas **13**, 103504 (2006).
[20]M. Keidar and I. D. Boyd, Appl. Phys. Lett. **87**, 121501 (2005).
[21]E. Fossum and L. King, IEEE Trans. Plasma Sci. **36**, 2088 (2008).
[22]A. Smirnov, Y. Raitses, and N. J. Fisch, Phys. Plasmas **14**, 057106 (2007).
[23]A. Fruchtman, R. Gueroult, and N. J. Fisch, Phys. Plasmas **20**, 073502 (2013).
[24]H. Date, Y. Ishimaru, and M. Shimozuma, Nucl. Instrum. Methods Phys. Res. B **207**, 373 (2003).